Assessing Guest Diffusivities in Porous Hosts from Transient Concentration Profiles

Lars Heinke,[1] Despina Tzoulaki,[1] Christian Chmelik,[1] Florian Hibbe,[1] Jasper M. van Baten,[2] Hyuna Lim,[3] Jing Li,[3] Rajamani Krishna,[2] and Jörg Kärger[1]

[1]*Faculty of Physics and Geosciences, Department of Interface Physics, University of Leipzig, Linnéstrasse 5, 04103 Leipzig, Germany*
[2]*Van't Hoff Institute for Molecular Sciences, University of Amsterdam, Nieuwe Achtergracht 166, 1018 WV Amsterdam, The Netherlands*
[3]*Department of Chemistry and Chemical Biology, Rutgers University, 610 Taylor Road, Piscataway, New Jersey 08854, USA*

(Received 22 September 2008; published 11 February 2009)

Using the short-chain-length alkanes from ethane to *n*-butane as guest molecules, transient concentration profiles during uptake or release (via interference microscopy) and tracer exchange (via IR microimaging) in Zn(tbip), a particularly stable representative of a novel family of nanoporous materials (the metal organic frameworks), were recorded. Analyzing the spatiotemporal dependence of the profiles provides immediate access to the transport diffusivities and self-diffusivities, yielding a data basis of unprecedented reliability for mass transfer in nanoporous materials. As a particular feature of the system, self- and transport diffusivities may be combined to estimate the rate of mutual passages of the guest molecules in the chains of pore segments, thus quantifying departure from a genuine single-file system.

DOI: 10.1103/PhysRevLett.102.065901 PACS numbers: 66.30.je, 66.30.Pa, 68.43.Jk

Owing to most recent significant developments in material sciences [1] and driven by the fascinating prospects of technical application [2], the diversity of nanoporous materials is continuously increasing [3]. Diffusion is among those processes which may decide about the technological performance of these materials [4–6]. Simultaneously, it is one of the most fundamental phenomena and the investigation of diffusion under confinement [7,8] is among the hot topics of current fundamental research. Thus, diffusion in nanoporous materials is addressed in numerous publications, with many of them developing theoretical concepts for the explanation of experimental data [9–12]. However, beginning with the application of the pulsed field gradient nuclear magnetic resonance to diffusion studies with zeolites [5,13,14], the experimental determination of reliable diffusivities in nanoporous host-guest systems proved to be far from trivial. In fact, in numerous cases "real" specimens of nanoporous material turned out to notably deviate from the ideal textbook structure, with the possibility that these deviations (pore blockage, cracks), rather than diffusion in the genuine pore space, become rate determining for the observed transport phenomena [15,16]. This constraint is of immediate impact on molecular modeling, since it is the experimental evidence which has to serve as the ultimate criterion of its validity.

Among the numerous techniques applied to diffusion measurement in nanoporous materials [5,6,14,17], only the recently introduced methods of interference microscopy [16,18–20] and IR microimaging [16] [supplementary material (SM) 1 and 2 [21]] are able to monitor transient concentration profiles and, hence, diffusion fluxes directly in the interior of individual nanoporous crystallites. To our knowledge, never before in any type of matter could diffusion-driven transient concentration profiles be observed with a similar wealth of information [22,23]. Moreover, by following tracer exchange, IR microimaging is also able to operate under (quasi-) equilibrium conditions. The virtue of these techniques, namely, to focus on a particular, isolated crystal, raises the problem that the number of adsorption or desorption cycles which could be performed with an individual crystal remained rather limited due to sample instabilities. Though to different extents, for most of the investigated specimens the transport parameters were eventually found to change with increasing cycle numbers. With the advent of Zn(tbip) (H_2tbip = 5-*tert*-butyl isophthalic acid) [24], a highly stable representative of the family of microporous metal organic frameworks (MOFs), we dispose of a nanoporous host system for which an essentially unlimited reproducibility in subsequent adsorption-desorption cycles could be observed. Zn(tbip) (see Fig. 1 and SM 4) is traversed by an array of parallel chains of pore segments in the direction of longitudinal crystal extension. The resulting one-dimensionality of diffusion and structural stability make MOFs of type Zn(tbip) excellent candidates for a systematic, experimentally founded investigation of the key features of mass transfer in nanoporous materials.

Altogether, more than 60 different adsorption and desorption runs with three different guest molecules (ethane, propane, and *n*-butane) and three runs of tracer exchange (between propane and deuterated propane at two different loadings) have been performed. All measurements were carried out at room temperature (298 K). The adsorption and desorption experiments were initiated by a stepwise variation of the pressure in the surrounding gas atmosphere which can be assumed to occur essentially instantaneously. For observing tracer exchange, after equilibration with the host system, the molecules in the surrounding atmosphere were replaced by their isotopes. Examples of the evolution

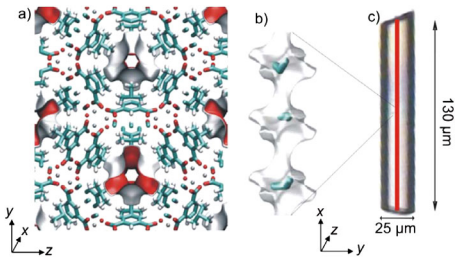

FIG. 1 (color online). Model representation (a),(b) and image (c) of the MOF Zn(tbip) under study. The atoms of the crystal framework and the one-dimensional pore structure. The side pockets are ordered like two three-leafed clover separated by windows of a diameter of 0.45 nm. The red (or gray) surface indicates the surface of the pores as perceived by the guest molecules. (c) Crystal under investigation. The red (or gray) line indicates that the profiles are recorded in the center of the crystal.

of the thus recorded concentration profiles are shown in Figs. 2 and 3, as well as in the SM 1 and 2. It is worthwhile mentioning that, following recent studies with notably poorer spatiotemporal resolution [25,26], it is only the introduction of IR microimaging by focal-plane array detection [27] that allowed the observation of the transient tracer exchange profiles of the quality shown in Fig. 2.

In all experiments, the boundary concentration does not immediately reach the equilibrium value. This indicates an additional transport resistance at the surface, i.e., a reduced surface permeability [28]. Reference to the underlying transport parameters has to take account, therefore, of both the intracrystalline diffusivities and surface permeabilities. Intracrystalline diffusivities are defined as factors of proportionality between particle fluxes and concentration gradients, surface permeabilities as factors of proportionality between particle fluxes and the difference between the actual boundary concentration and the concentration in equilibrium with the surrounding atmosphere [4,5,13,14] (see also SM 5). If observed under overall concentration gradients, they are referred to as ''transport''

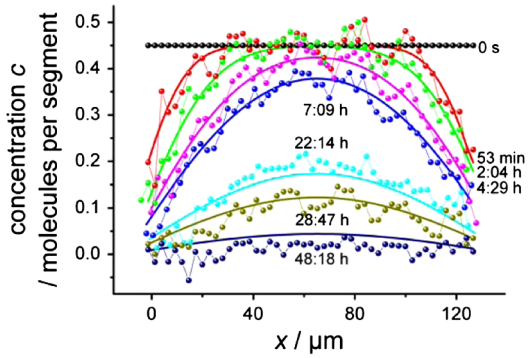

FIG. 2 (color online). Transient concentration profiles of deuterated propane in MOF Zn(tbip) during tracer exchange with the undeuterated isotope at an overall pressure of 60 mbar. Thin lines represent the best fits of the analytical expressions for tracer exchange with a constant surface permeability and diffusivity.

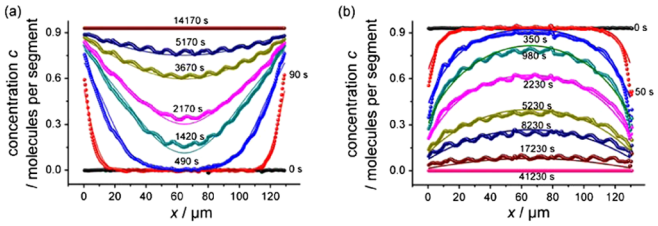

FIG. 3 (color online). Transient concentration profiles of propane in Zn(tbip) during adsorption [0 to 480 mbar (a)] and desorption [480 mbar to vacuum (b)]. The thin lines represents the best fits of the numerical solution with a concentration dependence of the surface permeability and the diffusivity provided by a Reed-Ehrlich ansatz.

diffusivities (permeabilities), if observed by tracer exchange, they are self- (or tracer exchange) diffusivities (permeabilities). The experimental accessible space scale exceeds the nanoscale (pore distance) of the material by several orders of magnitude so that the relevant relations of mass transfer end up in a continuous diffusion equation (Fick's 1st and 2nd laws, SM 5).

During tracer exchange, profile evolution is therefore controlled by a single value of the (tracer or self-) diffusivity and surface permeability (depending on the overall concentration), rather than on the (varying) concentration of labeled (or unlabeled) molecules. Figures 4(b) and 4(e) show the data which yield best fits between the measured curves and their theoretical prediction (full lines in Fig. 2, as well as in Fig. S4 [21]) by the standard relations of

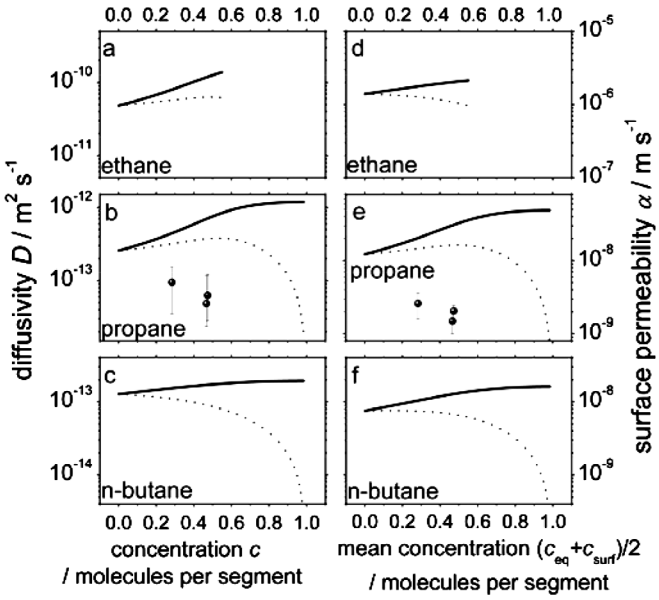

FIG. 4. Diffusivity (left) and surface permeability (right) of ethane, propane, and *n*-butane in Zn(tbip) as resulting as a best fit to the experimentally determined transient concentration profiles. The results from (nonequilibrium) uptake or release experiments are presented by full lines, the tracer exchange data by points. The corrected (MS) parameters used in the fitting procedure are indicated by dotted lines.

molecular uptake or release with constant diffusivities and surface permeabilities [5,29] (SM 6).

Under transient uptake and release, account has to be taken of a possible concentration dependence of both the intracrystalline (transport) diffusivity and the surface permeability. By means of the adsorption isotherm $c(p)$ (SM 3), the transport diffusivity can be related to a ''Maxwell-Stefan'' (MS, or ''corrected'') diffusivity D_0 by the relation [4,5,9]

$$D_T = \frac{\partial \ln p}{\partial \ln c} D_0. \tag{1}$$

The equilibrium concentrations $c(p)$ of propane and n-butane are found to follow a single-site-Langmuir isotherm with a maximum loading of one molecule per (channel) segment, while Configurational-Bias Monte Carlo (CBMC) simulations show that ethane occupies two different adsorption sites (SM 3,4).

By considering only nearest-neighbor interaction on a surface of equal adsorption sites, Reed and Ehrlich derived the following analytical expression of the concentration dependence of diffusion [30–32]:

$$D_0 = D_0(0) \frac{(1+\varepsilon)^{z-1}}{(1+\varepsilon/\phi)^z}, \tag{2}$$

with

$$\varepsilon = \frac{(\beta - 1 + 2\theta)\phi}{2 - 2\theta}, \tag{3}$$

$$\beta = \sqrt{1 - 4\theta(1-\theta)(1-1/\phi)}. \tag{4}$$

z is the coordination number (number of nearest neighbors), which equals 2 for one-dimensional systems. θ denotes the occupancy, i.e., the concentration divided by the maximum concentration, $c/c_{\max}$. Most remarkably (and conveniently), over the total range of concentrations the diffusivity is found to be determined by only two parameters, namely, the MS diffusivity $D_0(0)$ at zero loading (coinciding with the transport and self-diffusivity at this loading) and the ''interaction'' parameter ϕ (>1 for repulsive and <1 for attractive interaction, see SM 5). In the limiting case of simple hard-core interaction ($\phi = 1$), Eq. (2) simplifies to the lattice-gas relation $D_0 \sim (1-\theta)$ [33,34]. In many studies the observed concentration dependencies were found to nicely follow an analytical expression provided by Eqs. (1)–(4) [12,32]. Using this ansatz for both the diffusivities and surface permeabilities, we attained an excellent reproduction of the transient concentration profiles also in our experiments. This is visualized by the full lines in the representations of the transient concentration profiles. They have been calculated with the diffusivities and surface permeabilities with the concentration dependences resulting by inserting the fitting parameters summarized in Table I into Eqs. (2) to (4) by a numerical solution of the diffusion equation [29,35]. Most importantly, this agreement is demonstrated to exist for both adsorption and desorption, confirming reproducibility and reversibility of the measurements. Figure 4 summarizes the concentration dependences of the transport diffusivities and surface permeabilities determined in our studies. As well included are the corresponding ''corrected'' quantities resulting from the respective adsorption isotherms via Eq. (1).

The simultaneous measurement of transport diffusion and self-diffusion allows an assessment of up to which extent mass transfer in the chain of pore segments in Zn(tbip) is subject to single-file diffusion [36–39]. In a perfect single-file system of N sites (pore segments) the effective self-diffusivity of tracer exchange is known to be exceeded by $D_0(0)$ by a factor of $N\theta/(1-\theta)$ [40–42]. With crystal lengths ≥ 100 μm and a site distance of $\lambda \approx 1$ nm, the resulting factors dramatically exceed the experimental values [Fig. 4(b)] of about 2 and 5 for $\theta = 0.28$ and 0.48, respectively. Hence, within the chains of pore segments in the crystals under study the propane molecules must definitely have the possibility of mutual passages. The passage rate Γ of a particular pair of adjacent molecules is related to the tracer (or self-) diffusivity D^* by the simple random-walk expression

$$D^* = l^2 \Gamma \tag{5}$$

where $l(\approx\lambda/\theta)$ denotes the mean distance between adjacent molecules. With the simplifying assumption that a jump attempt towards an empty segment is always successful, while it is only successful with the probability p if this segment is occupied, the passage rate may be correlated by the expression

$$\Gamma = \frac{p(1-\theta)}{2\tau} \tag{6}$$

with the mean time τ between jump attempts. Inserting Eq. (6) into (5) yields

$$D^* = \frac{\lambda^1}{2\tau} \frac{p(1-\theta)}{\theta^2} = D_0(0) \frac{p(1-\theta)}{\theta^2}, \tag{7}$$

TABLE I. Reed-Ehrlich parameters used for the construction of the concentration dependencies of the transport diffusivities and surface permeabilities following Eqs. (1)–(4), yielding best fits to the recorded concentration profiles.

Guest molecule	$D_0(0)$	ϕ_D	$\alpha_0(0)$	ϕ_α	Standard deviation between measured and recalculated concentrations profiles
Ethane	5.2×10^{-11} m^2 s^{-1}	2.6	1.3×10^{-6} m s^{-1}	2.1	4.4%
Propane	2.4×10^{-13} m^2 s^{-1}	4.9	2.7×10^{-8} m s^{-1}	2.9	3.8%
n-butane	1.3×10^{-13} m^2 s^{-1}	1.5	7.6×10^{-9} m s^{-1}	2.1	3.1%

from which one obtains passage probabilities of $p = 5.5 \times 10^{-2}$ and 8.8×10^{-2} for $\theta = 0.28$ and 0.48, respectively. The increase of p with increasing loading may be referred to the repulsive interaction of the diffusants which, in the chosen model approach, has already been found to give rise to values >1 for the fitting parameter ϕ of concentration dependence.

On applying the concentration dependence of the Reed-Ehrlich model, we have made use of a most versatile option of representing a large spectrum of possible concentration dependences by a minimum of free parameters. The measured concentration profiles are in excellent agreement with the corresponding solutions of the diffusion equation with the thus described diffusivities and permeabilities (Table I). However, with the successful application of the concentration dependence as following from the Reed-Ehrlich model, the model can clearly not automatically be assumed to adequately represent the microdynamic features of mass transfer. The substantial data spectrum covering three different chain lengths and a large range of concentrations is rather expected to give rise to the application of more refined techniques of molecular modeling and to their comparison with experimental evidence.

Financial support by Deutsche Forschungsgemeinschaft (R. K., International Research Group ''Diffusion in Zeolites'' and International Research Training Group ''Diffusion in Porous Materials''), Max-Buchner-Forschungsstiftung, INDENS Marie-Curie program, and Studienstiftung des Deutschen Volkes are gratefully acknowledged.

[1] B. Wang *et al.*, Nature (London) **453**, 207 (2008).
[2] M. Eddaoudi *et al.*, Science **295**, 469 (2002).
[3] S. Kitagawa, R. Kitaura, and S. Noro, Angew. Chem., Int. Ed. **43**, 2334 (2004).
[4] R. Krishna and J. M. van Baten, Chem. Eng. Sci. **63**, 3120 (2008).
[5] J. Kärger and D. M. Ruthven, *Diffusion in Zeolites and Other Microporous Solids* (Wiley & Sons, New York, 1992).
[6] N. Y. Chen, T. F. Degnan, and C. M. Smith, *Molecular Transport and Reaction in Zeolites* (Wiley-VCH, New York, 1994).
[7] Q. H. Wei, C. Bechinger, and P. Leiderer, Science **287**, 625 (2000).
[8] L. A. Clark, G. T. Ye, and R. Q. Snurr, Phys. Rev. Lett. **84**, 2893 (2000).
[9] H. Jobic and D. Theodorou, Microporous Mesoporous Mater. **102**, 21 (2007).
[10] E. Beerdsen, D. Dubbeldam, and B. Smit, Phys. Rev. Lett. **96**, 044501 (2006).
[11] R. Haberlandt, S. Fritzsche, and H. L. Vörtler, in *Handbook of Surfaces and Interfaces of Materials*, edited by H. S. Nalwa (Academic Press, New York, 2001), Vol. 5, p. 357.
[12] R. Krishna and J. M. v. Baten, Microporous Mesoporous Mater. **109**, 91 (2008).
[13] J. Kärger, *Leipzig, Einstein, Diffusion* (Leipziger Universitätsverlag, Leipzig, 2007).
[14] D. M. Ruthven and M. F. M. Post, in *Introduction to Zeolite Science and Practice*, edited by H. van Bekkum, E. M. Flanigen, P. A. Jacobs, and J. C. Jansen (Elsevier, Amsterdam, 2001), p. 525.
[15] C. Chmelik, P. Kortunov, S. Vasenkov, and J. Kärger, Adsorption **11**, 455 (2005).
[16] L. Heinke *et al.*, Chem. Eng. Technol. **30**, 995 (2007).
[17] H. Jobic, J. Kärger, and M. Bee, Phys. Rev. Lett. **82**, 4260 (1999).
[18] J. Kärger *et al.*, Angew. Chem., Int. Ed. **45**, 7846 (2006).
[19] U. Schemmert *et al.*, Europhys. Lett. **46**, 204 (1999).
[20] D. Tzoulaki *et al.*, Angew. Chem., Int. Ed. **47**, 3954 (2008).
[21] See EPAPS Document No. E-PRLTAO-102-059907 for supplementary material on infrared microimaging, recorded concentration profiles, adsorption isotherms, Monte Carlo simulations, mass transfer in nanoporous materials, and the Reed-Ehrlich model. For more information on EPAPS, see http://www.aip.org/pubservs/epaps.html.
[22] W. Jost, *Diffusion in Solids, Liquids and Gases* (Academic Press, New York, 1960).
[23] P. Heitjans and J. Kärger, *Diffusion in Condensed Matter: Methods, Materials, Models* (Springer, Berlin, Heidelberg, 2005).
[24] L. Pan *et al.*, J. Am. Chem. Soc. **128**, 4180 (2006).
[25] D. R. Kodali, D. M. Small, J. Powell, and K. Krishnan, Appl. Spectrosc. **45**, 1310 (1991).
[26] E. Lehmann *et al.*, J. Am. Chem. Soc. **124**, 8690 (2002).
[27] Y. Roggo, A. Edmond, P. Chalus, and M. Ulmschneider, Anal. Chim. Acta **535**, 79 (2005).
[28] L. Heinke, P. Kortunov, D. Tzoulaki, and J. Kärger, Phys. Rev. Lett. **99**, 228301 (2007).
[29] J. Crank, *The Mathematics of Diffusion* (Clarendon Press, Oxford, 1975).
[30] D. A. Reed and G. Ehrlich, Surf. Sci. **102**, 588 (1981).
[31] R. Krishna, D. Paschek, and R. Baur, Microporous Mesoporous Mater. **76**, 233 (2004).
[32] G. K. Papadopoulos, H. Jobic, and D. N. Theodorou, J. Phys. Chem. B **108**, 12748 (2004).
[33] P. Kortunov *et al.*, J. Am. Chem. Soc. **129**, 8041 (2007).
[34] K. W. Kehr, K. Mussawisade, G. M. Schütz, and T. Wichmann, in *Diffusion in Condensed Matter-Methods, Materials, Models*, edited by P. Heitjans and J. Kärger (Springer, Berlin, 2005), p. 975.
[35] L. Heinke and J. Kärger, New J. Phys. **10**, 023035 (2008).
[36] K. Hahn, J. Kärger, and V. Kukla, Phys. Rev. Lett. **76**, 2762 (1996).
[37] C. Lutz, M. Kollmann, and C. Bechinger, Phys. Rev. Lett. **93**, 026001 (2004).
[38] M. Kollmann, Phys. Rev. Lett. **90**, 180602 (2003).
[39] F. Marchesoni and A. Taloni, Chaos **17**, 043112 (2007).
[40] S. Vasenkov and J. Kärger, Phys. Rev. E **66**, 052601 (2002).
[41] C. Rödenbeck and J. Kärger, J. Chem. Phys. **110**, 3970 (1999).
[42] P. H. Nelson and S. M. Auerbach, J. Chem. Phys. **110**, 9235 (1999).

Supplementary Material 1: Infrared micro-imaging

We are going to describe very briefly the used IR micro-imaging device. More details of FTIR spectroscopy and the technique can be found in references [1-7].
The Fourier Transform Infrared (FTIR) microscope *Bruker Hyperion 3000* consists of a spectrometer *Bruker Vertex 80v* and a microscope with a Focal Plane Array (FPA) detector (Figure S 1).
The novel FPA detector consists of an array of 128 × 128 single detectors with a size of 40 µm × 40 µm each. By means of a 15x objective, a resolution of 2.7 µm × 2.7 µm is gained in the focal plane. The beam is focussed with a maximum beam width of 23.5 °.
Each single detector of the FPA records an IR signal. The intensity of the IR light as a function of the wavelength, i.e. the transmission spectrum, is determined by means of the spectrometer by using Fourier transformation.
All molecules with a dipole moment absorb photons of a specific energy[5, 6]. This means that the absorption bands have a specific wave number (reciprocal wave length). Therefore, different molecules can be distinguished by their different absorption bands (Figure S 2).

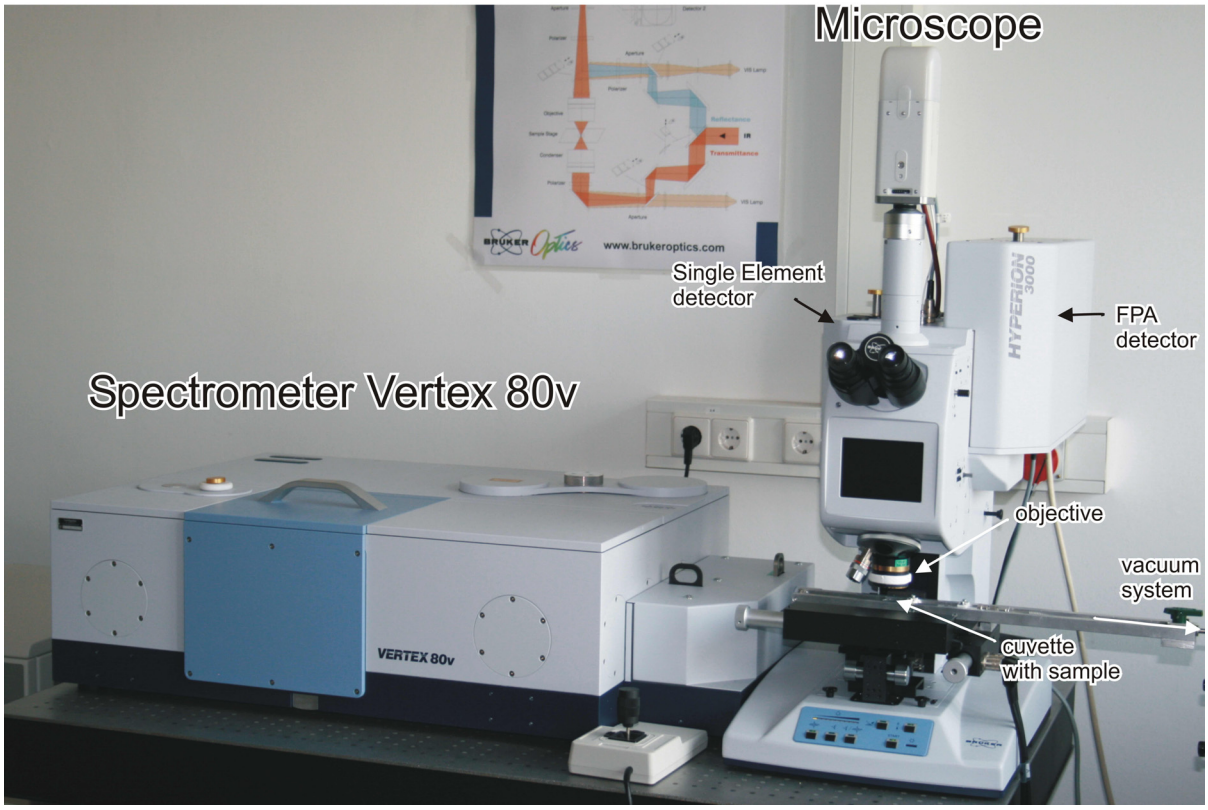

Figure S 1 Picture of the IR micro-imaging *Bruker Hyperion 3000* which consists of a spectrometer and the microscope with optics and the detectors. The main part of the spectrometer is a Michelson interferometer.

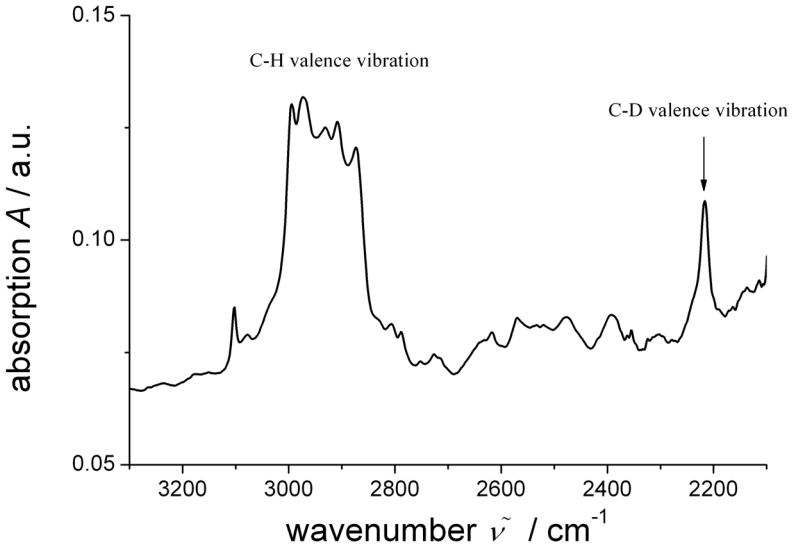

Figure S 2:IR absorption spectra of deuterated propane in MOF Zn(tbip). The absorption band of the C-D valence vibrations are clearly distinguished from the C-H valence vibrations of the crystal framework.
The absorption spectrum is the negative logarithm of the ratio of the transmission spectrum of the sample and of the background.

As a consequence of Lambert-Beer's law, the concentration of adsorbed molecules is proportional to the absorption band. Therefore, a two-dimensional concentration profile of the adsorbed molecules with a resolution up to 2.7 µm can be recorded with this IR micro-imaging device (Figure S3 and Figure S4)

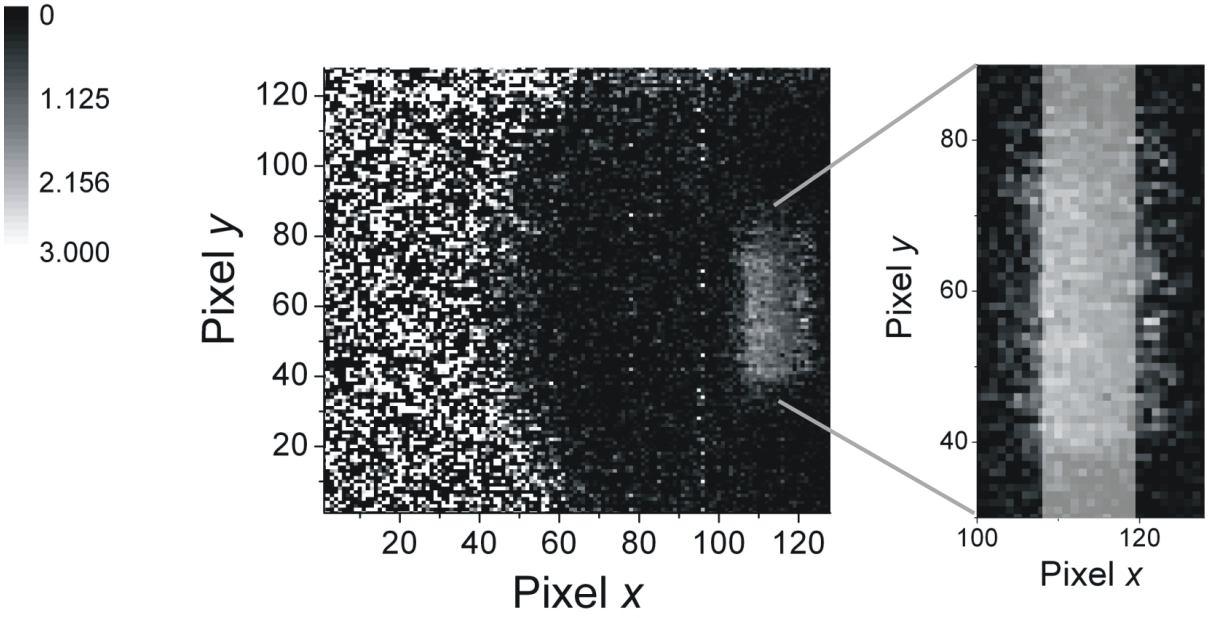

Figure S3: Two-dimensional profile of the C-D absorption band recorded by IR micro-imaging. The gray scale displays the intensity of the C-D band (from 0 to 3 a.u.). The crystal is equilibrated with the surrounding atmosphere of 60 mbar deuterated propane. The bright bar represents the region which yields the profiles pictured in Figure S4.
The scattering on the left side of the picture is caused by the "bad" illumination of the detector caused by its large size.

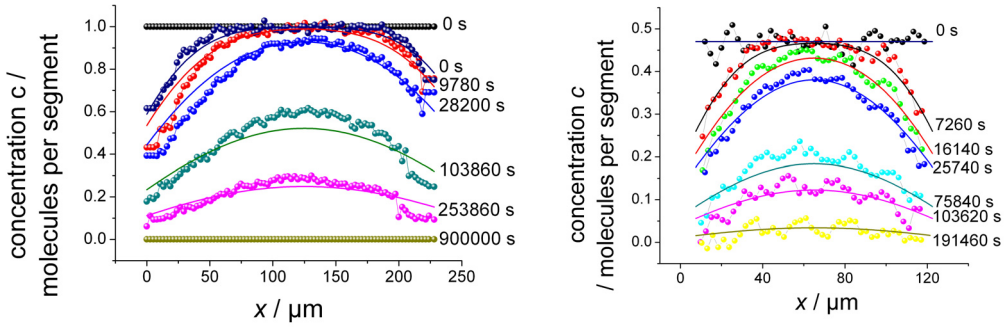

Figure S4: Transient concentration profiles of deuterated propane in MOF Zn(tbip) during tracer exchange with the undeuterated isotope at an overall pressure of 30 mbar (a) and 60 mbar (b). Thin lines represent the best fits of the analytical expressions for tracer exchange with a constant surface permeability and diffusivity.

References

[1] M. Hermann, W. Niessen, and H. G. Karge, in *Catalysis by Microporous Materials*, edited by H. K. Beyer, H. G. Karge, I. Kiricsi and J. B. Nagy (Elsevier, Amsterdam, 1995), p. 131.

[2] H. G. Karge, W. Niessen, and H. Bludau, Applied Catalysis A-General. **146**, 339 (1996).

[3] W. Niessen and H. G. Karge, Microporous Mater. **1**, 1 (1993).

[4] C. Chmelik, PhD. Thesis (2007).

[5] R. J. Bell, *Introductory Fourier Transform Spectroscopy* (Academic Press, New York, 1972).

[6] P. R. Griffiths and J. A. des Haseth, *Fourier Transform Infrared Spectrometry* (J. Wiley & Sons, New York, 1986).

[7] Bruker-Optics, *User Manual Vertex 80v and User Manual Hyperion* (Bruker Optik GmbH, Ettlingen, 2006).

Supplementary Material 2: Concentration profiles recorded by Interference Microscopy

A Jenamap p dyn (Carl Zeiss GmbH) interference microscope equipped with an interferometer of the Mach-Zehnder type is the basic technique used for the purpose of this study. Its high spatial resolution (0.5 µm × 0.5 µm), together with a time resolution of 10 s (determined by implemented phase shifts for phase determination), enabled us to record the transient concentration profiles of the guest molecules with high accuracy. On the basis of this technique, we correlate the optical path length of the beam passing through the crystal under study with the refractive index of the medium (crystal) and with the actual intracrystalline concentration. The first quantity is measured, the latter is determined. A fully detailed description of the method can be found in refs. [1] and [2]. All experiments are performed with the same crystal (see figure 1).

Transient concentration profiles of ethane in MOF Zn(tbip)

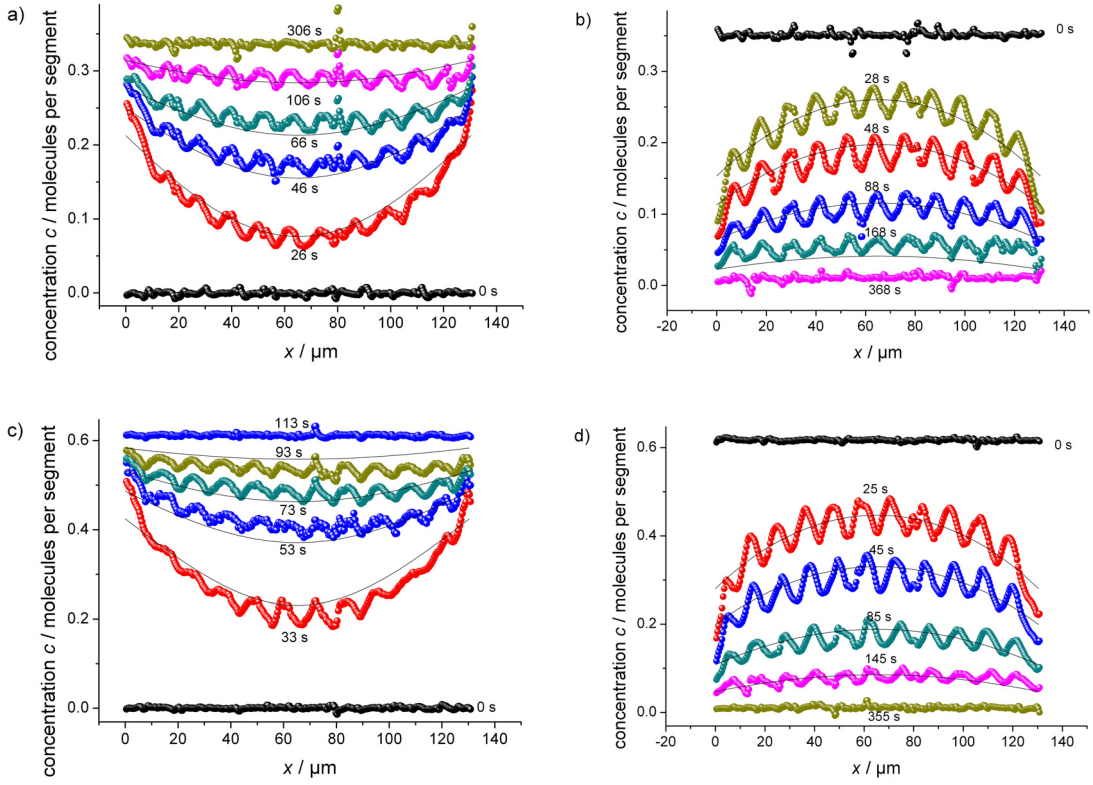

Figure S 5: Transient concentration profiles of ethane in MOF Zn(tbip). The pressure steps are from 0 to 255 mbar (a), from 255 mbar to 0 (b), from 0 to 734 mbar (c) and from 734 mbar to 0 (d). The symbols are recorded by IFM. The thin lines represent the numerical solutions of the corresponding diffusion equations with a concentration dependence of the diffusivities and surface permeabilities as provided by the two-parameter ansatz of the Reed-Ehrlich model which yield the best fist to the experimental data (see Table 1).
The standard deviations are mainly caused by the waves on the recorded concentration profiles which are generated by partial reflection at the crystal faces. Note that, e.g., in the case of propane, more than 200 concentration profiles recorded during more than 20 different adsorption and desorption experiments have been described with not more than 4 parameters.

Transient concentration profiles of propane in MOF Zn(tbip)

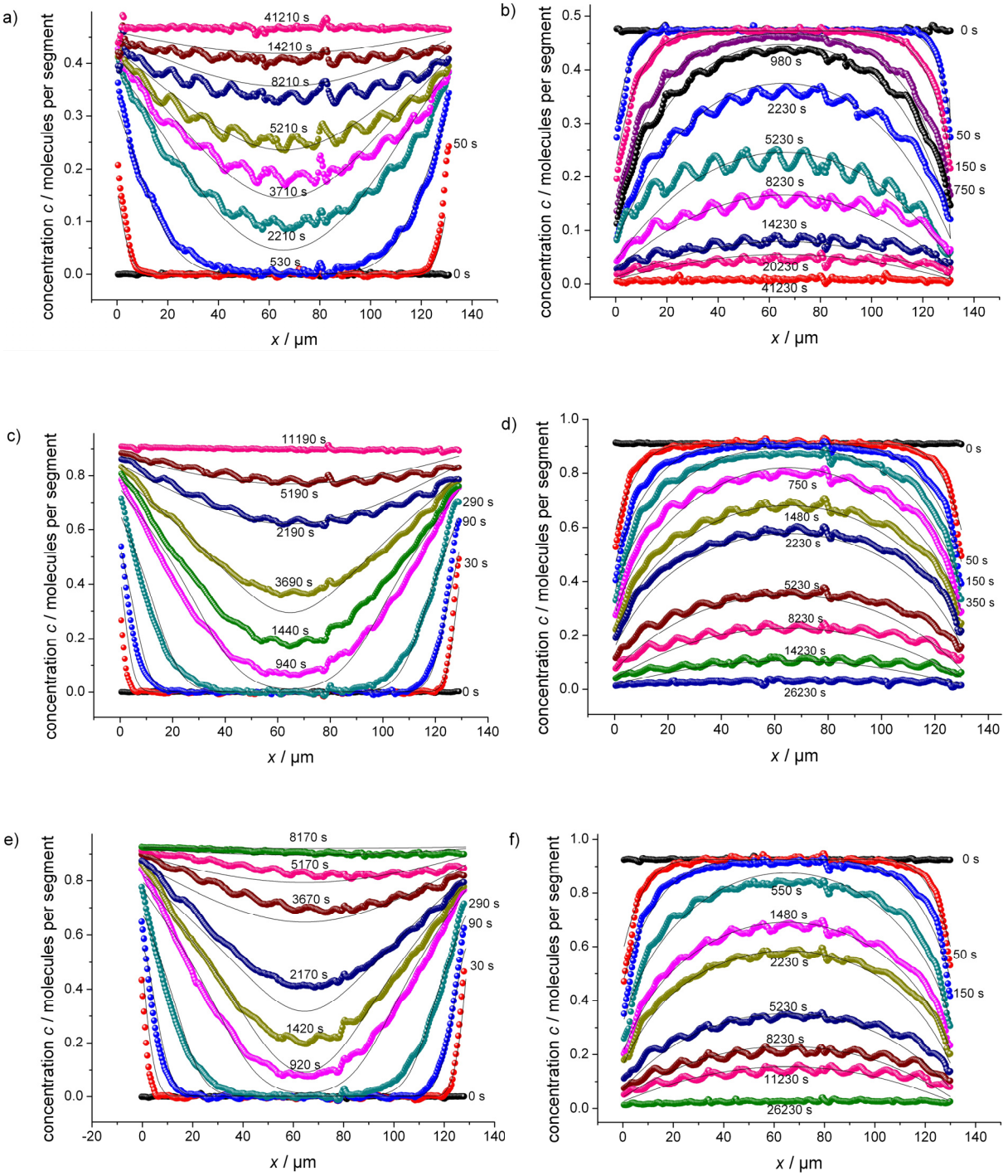

Figure S 6: Example of concentration profiles of propane in MOF Zn(tbip). The pressure steps are from 0 to 60 mbar (a), from 60 mbar to 0 (b), from 0 to 680 mbar (c), from 680 mbar to 0 (d), from 0 to 855 mbar (e) and from 855 mbar to 0 (f). The symbols are recorded by IFM. The thin lines represent the numerical solutions of the corresponding diffusion equations with a concentration dependence of the diffusivities and surface permeabilities as provided by the two-parameter ansatz of the Reed-Ehrlich model which yield the best fist to the experimental data (see Table 1).

Transient concentration profiles of n-butane in MOF Zn(tbip)

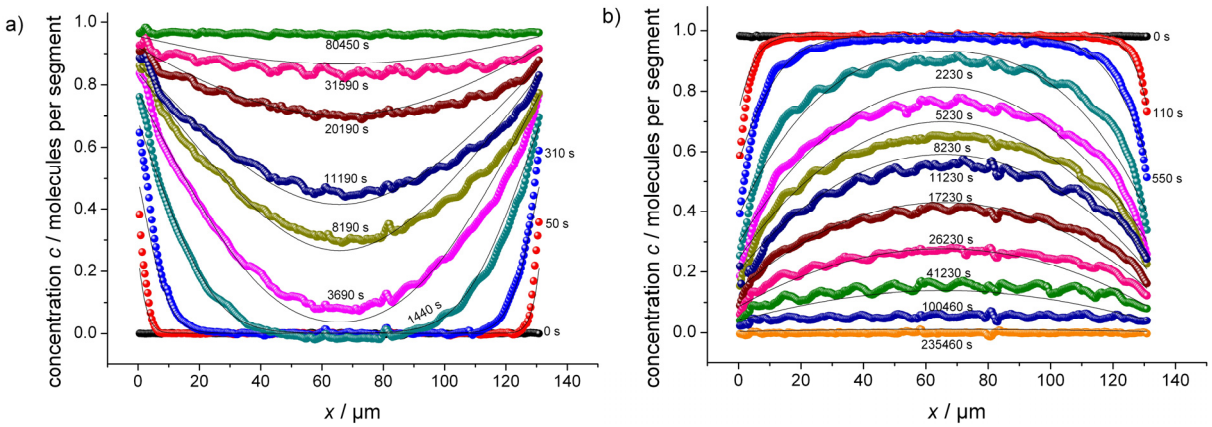

Figure S 7: Concentration profiles of n-butane in MOF Zn(tbip). The pressure steps are from 0 to 318 mbar (a) and from 318 mbar to 0 (b). The symbols are recorded by IFM. The thin lines represent the numerical solutions of the corresponding diffusion equations with a concentration dependence of the diffusivities and surface permeabilities as provided by the two-parameter ansatz of the Reed-Ehrlich model which yield the best fist to the experimental data (see Table 1).

References

1. U. Schemmert, J. Kärger, J. Weitkamp, *Microporous Mesoporous Mater.* **32,** 101 (1999).

2. J. Kärger *et al.*, *Angew. Chem. Int. Ed.* **45**, 7846 (2006).

Supplementary Material 3: Adsorption isotherms recorded by IFM and IRM

The adsorption isotherm is measured by means of infrared and interference microscopy at a temperature of 298 K. The obtained data are rescaled by means of the adsorption isotherms determined with CB Monte Carlo simulations (see Supplementary Material 4).

The shape of the experimental data can be described by a single-site Langmuir isotherm,

$$c = \frac{c_{sat} \cdot b \cdot p}{1 + b \cdot p}.$$

The Langmuir parameter b is determined to 0.00205 $mbar^{-1}$ for ethane (Figure S 8a) and to 0.015 $mbar^{-1}$ for propane (Figure S 8b).

Since the mass transfer of n-butane is very slow, only one adsorption/desorption experiment was performed. It is, therefore, not possible to determine the isotherm. So, the values determined by CBMC simulations are used ($b_{n\text{-butane}} = 0.77$ $mbar^{-1}$). The equilibrium loading at 318 mbar n-butane is close to the saturation loading. Therefore, small changes of the Langmuir parameter b do not affect the concentration.

There are six (channel) segments in each unit cell (figure S11 and S12), so a concentration of 1 molecule per segment corresponds to 6 molecules per unit cell.

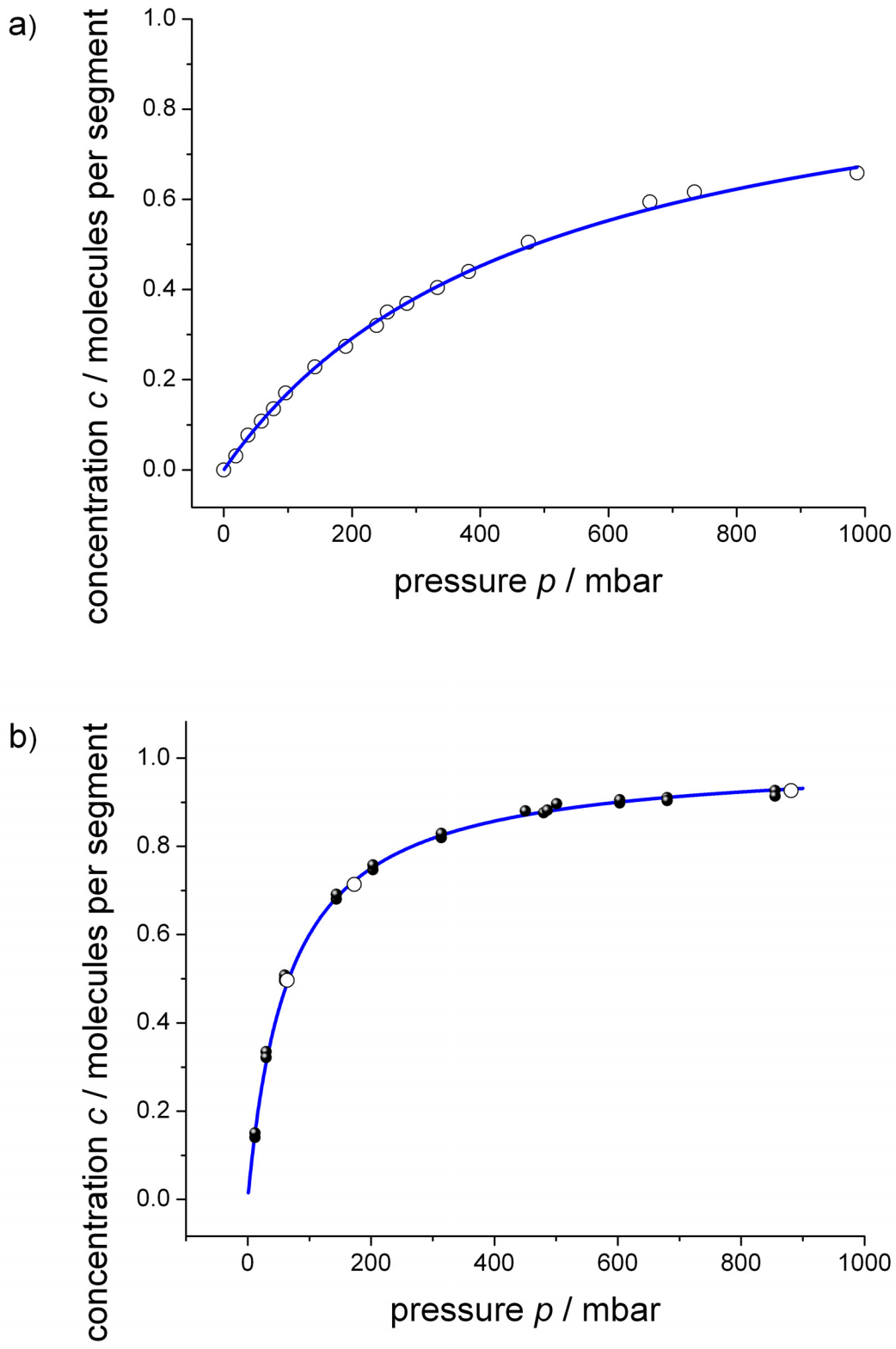

Figure S 8: Adsorption isotherm of ethane (a) and propane (b). The spheres are recorded by interference microscopy and the open circles by infrared microscopy. The thick blue lines indicates the best fit with a single-site-Langmuir isotherm.

Supplementary Material 4: Molecular Simulation methodology and simulation results

Monte Carlo simulation methodology

The structural information for Zn(tbip) simulations have been taken from Pan et al.[1]. The structure data file we used is available on our website [3]. The framework structure, and the pore (energy) landscapes are presented in Figures S9, S10, S11, and S12. One unit cell of Zn(tbip) contains a total of six channel segments.

The adsorption isotherms were computed using Monte Carlo (MC) simulations in the grand canonical (GC) ensemble. The united atom force field for alkanes, developed by Dubbeldam et al. [4], is used to describe alkane-alkane, Lennard-Jones, interactions. For alkane-alkane interactions the tabulated force fields are available in Dubbeldam et al. [4]; the potential for the n-alkanes includes bond stretching, bending, and torsion.

The Zn(tbip) framework was considered to be rigid in the simulations. For the atoms in the guest metal organic framework, the generic UFF [5] and DREIDING [6] force fields were used. The Lennard-Jones parameters are given in Table S1. The Lorentz-Berthelot mixing rules were applied for calculating σ and $\tilde{\varepsilon}/k_B$ for guest-host interactions. For simulations with linear and branched alkanes with two or more C atoms, the Configurational-Bias Monte Carlo (CBMC) simulation technique [7, 8] was employed. The beads in the chain are connected by harmonic bonding potentials. A harmonic cosine bending potential models the bond bending between three neighboring beads, a Ryckaert-Bellemans potential controls the torsion angle. The beads in a chain separated by more than three bonds interact with each other through a Lennard-Jones potential. The Lennard-Jones potentials are shifted and cut at 12 Å. The CBMC simulation details have been given in detail elsewhere [4, 7-9].

The CBMC simulations were performed using the BIGMAC code developed by T.J.H. Vlugt[10] as basis.

The molecules investigated in the present study are ethane (C2), propane (C3), and n-butane (nC4).

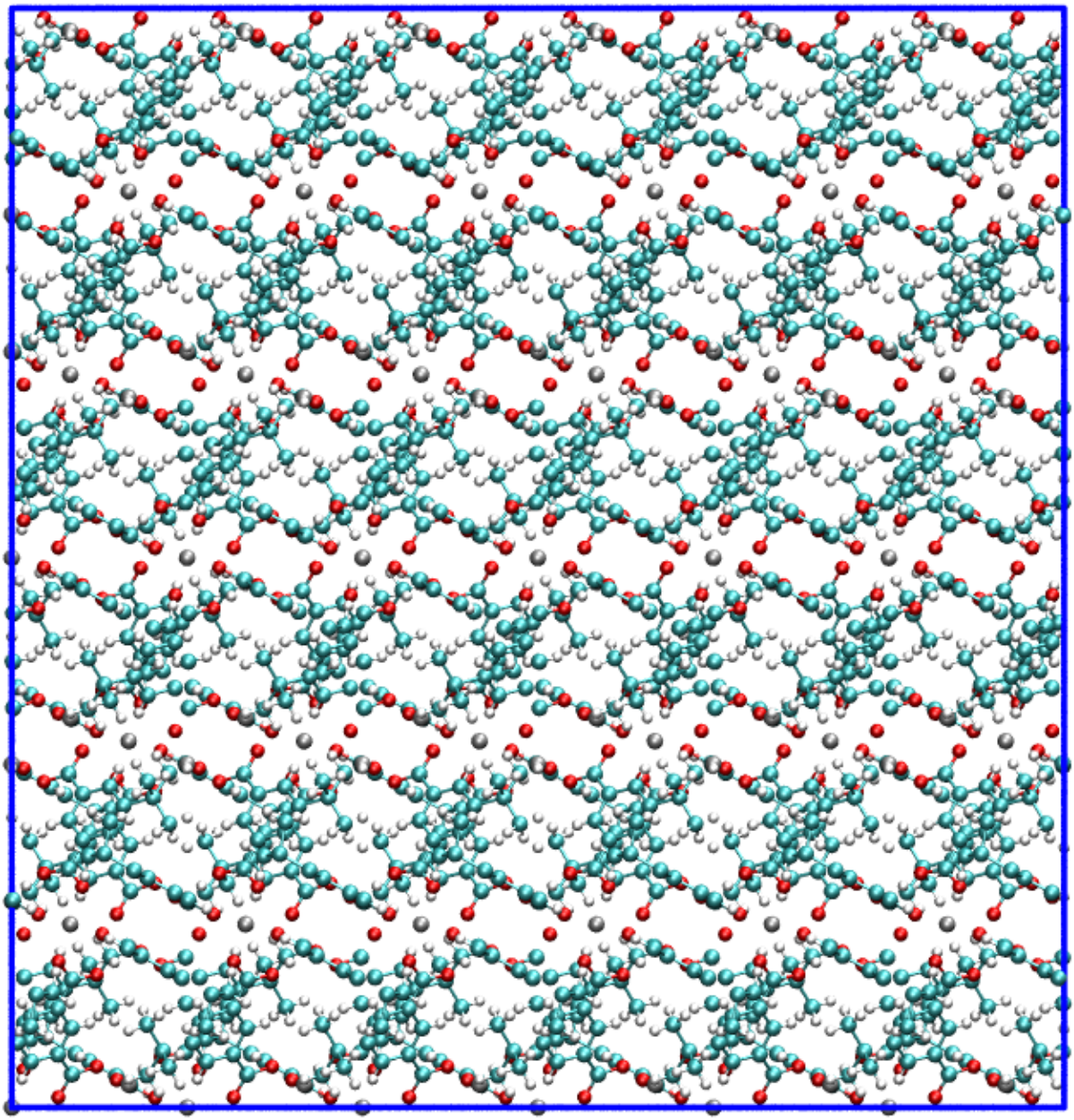

Figure S9. Sideways view of Zn(tbip) framework structure.

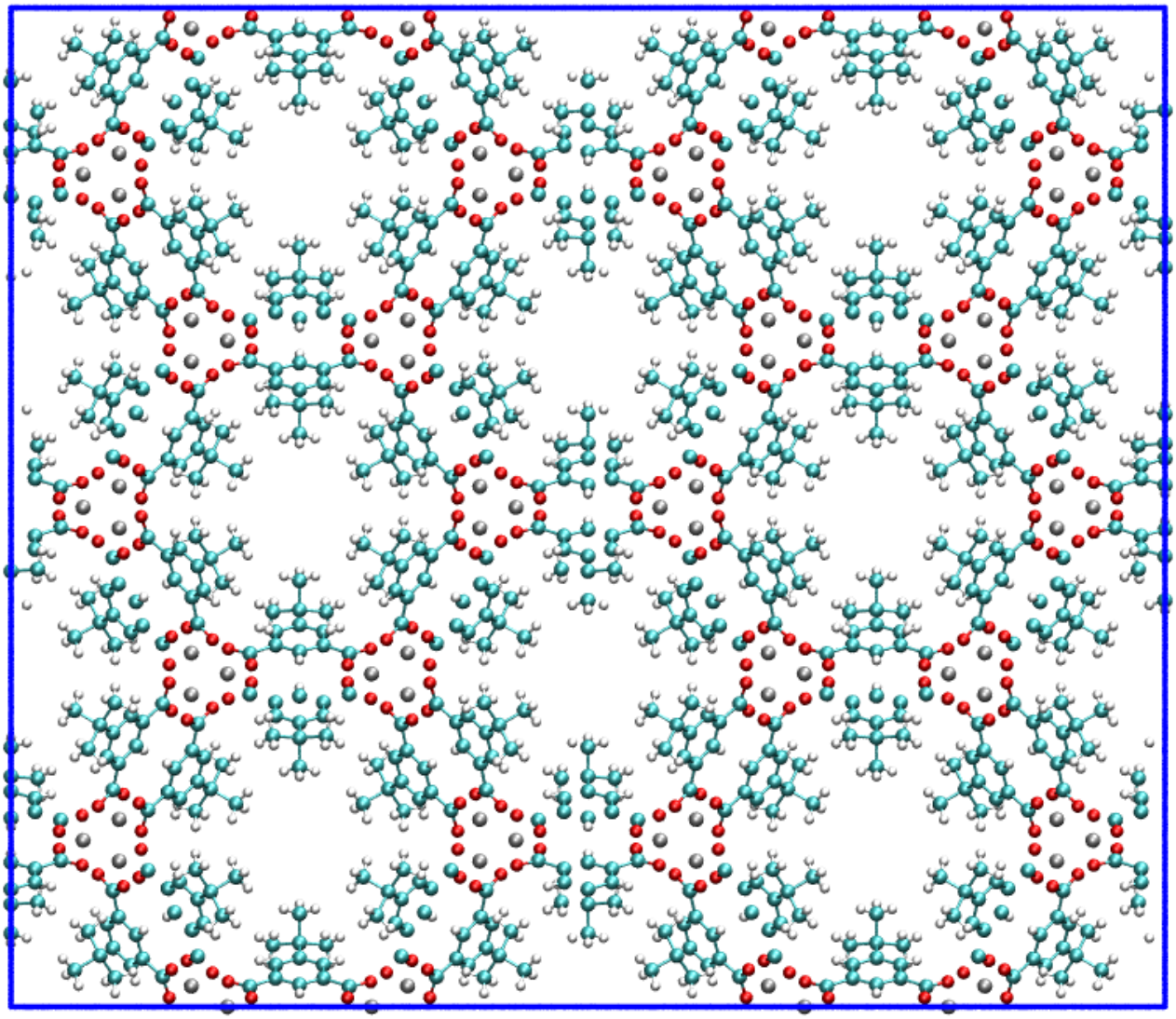

Figure S10. Head-on view of Zn(tbip) framework structure.

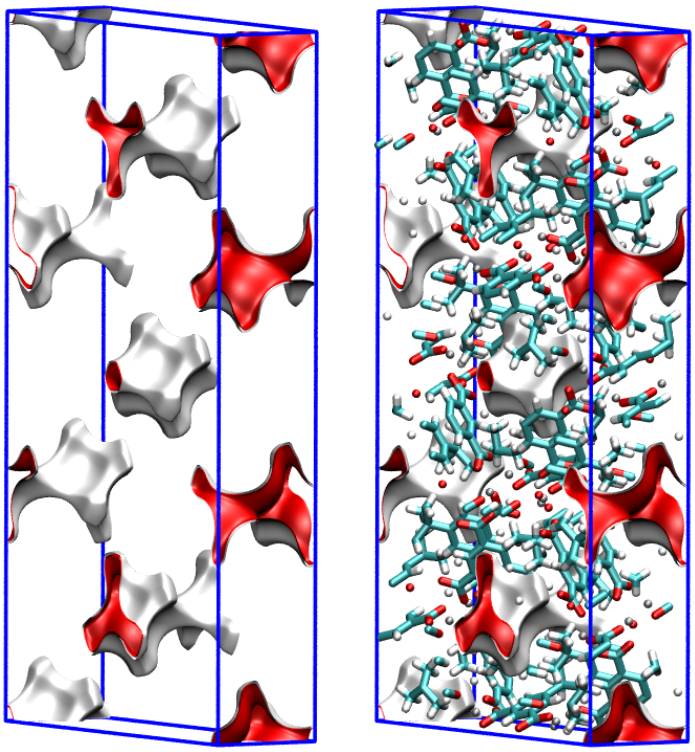

Figure S11. Perspective view of one unit cell of Zn(tbip), shown along with the pore energy landscapes. There are six (channel) segments in each unit cell.

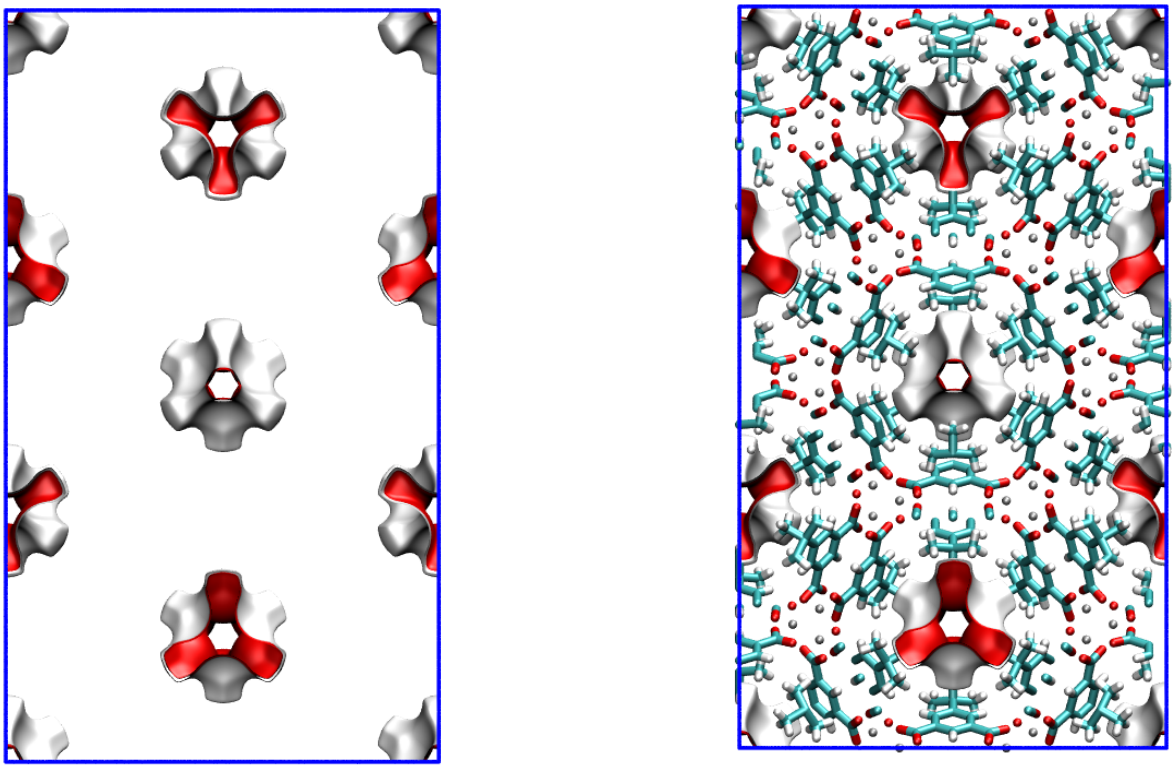

Figure S12. Head-on view of one unit cell of Zn(tbip), shown along with the pore energy landscapes.

Simulation results for the isotherms

The CBMC simulation results for the isotherms of ethane (C2), propane (C3), and n-butane (nC4) are shown in Figures S5, S6 and S7. The loadings are presented as the number of molecules per channel segment. For all three molecules investigated a saturation loading of 1 molecule per channel segment were used for fitting purposes. These values were also used to scale the experimental data, that were available only in arbitrary units for the loadings. Shown in Figures S8, S9 and S10 are snapshots showing the location of molecules within a channel containing eight segments.

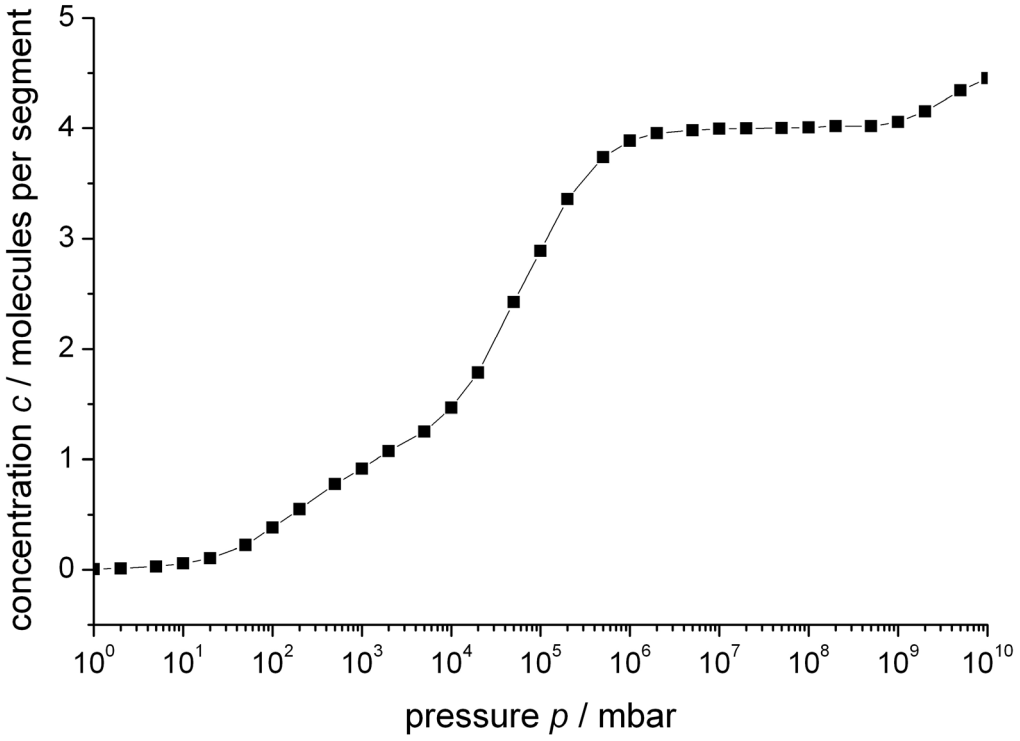

Figure S13. Isotherm of ethane determined from CBMC simulations. Both adsorption sites are occupied

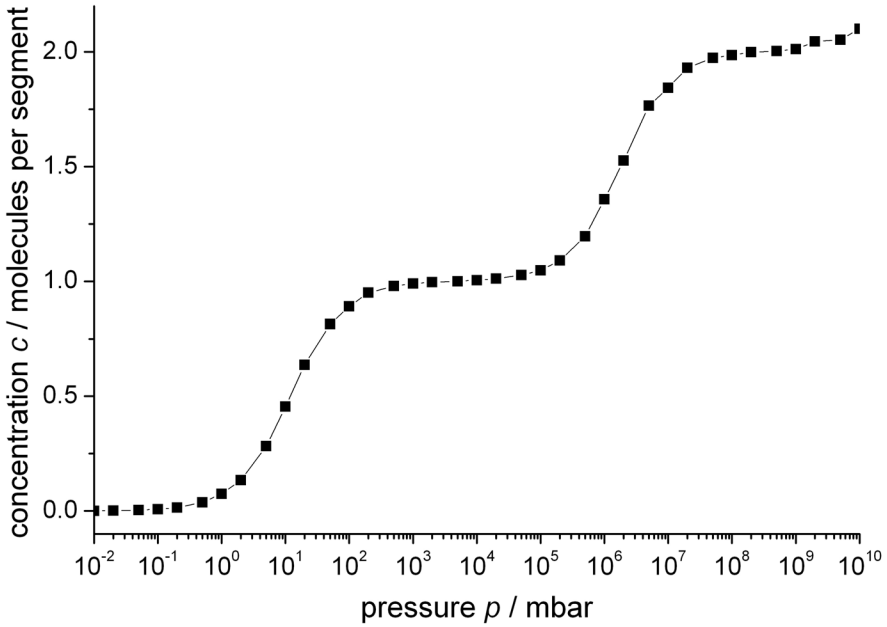

Figure S14. Isotherm of propane determined from CBMC simulations. The isotherm in the pressure range below 1000 mbar can be described with a single-site Langmuir isotherm with an equilibrium loading of 1 molecule per segment.

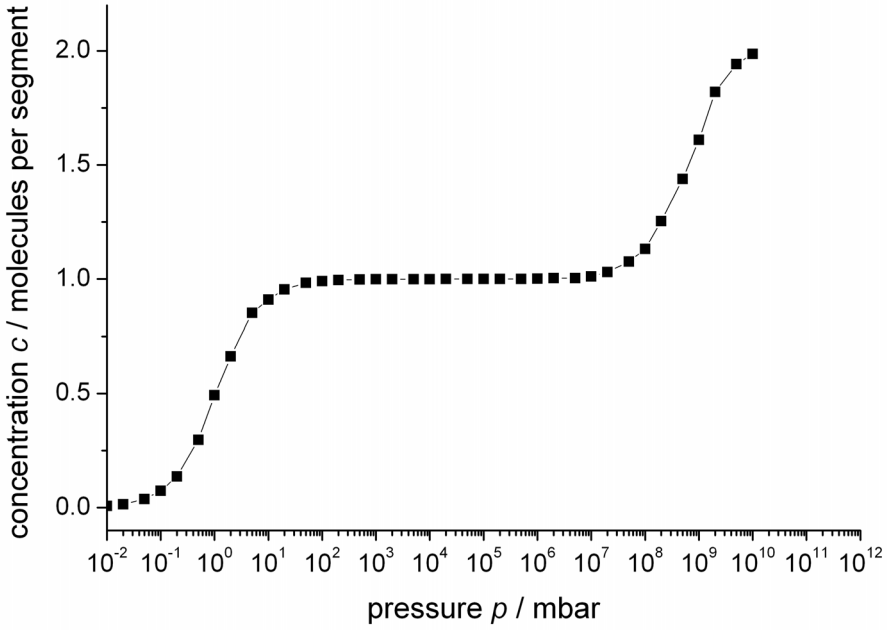

Figure S15. Isotherm of n-butane determined from CBMC simulations. The isotherm in the pressure range below 1000 mbar can be described with a single-site Langmuir isotherm with an equilibrium loading of 1 molecule per segment.

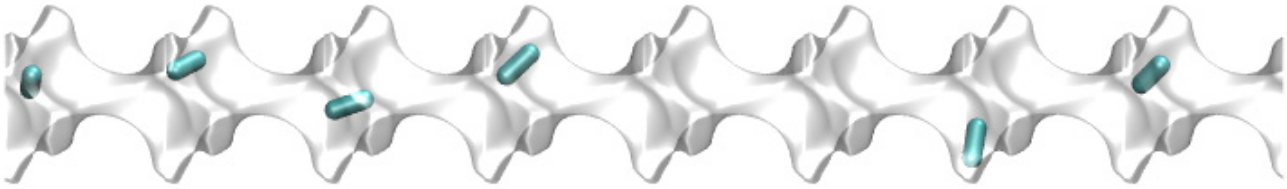

Figure S16. Snapshots showing the location of ethane (C2) molecules within the 1D pore landscapes of Zn(tbip) determined from CBMC simulations. The total loading is 4 molecules per unit cell.

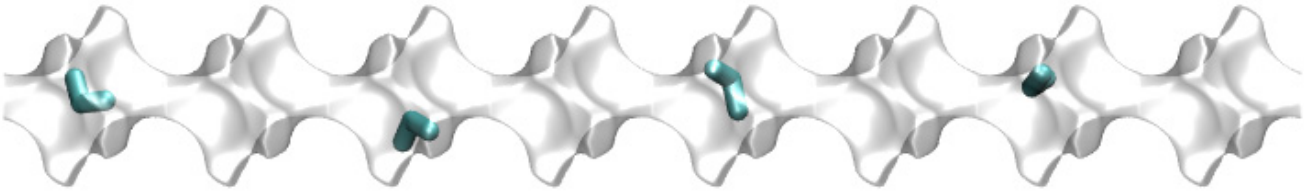

Figure S18. Snapshots showing the location of propane (C3) molecules within the 1D pore landscapes of Zn(tbip) determined from CBMC simulations. The total loading is 4 molecules per unit cell

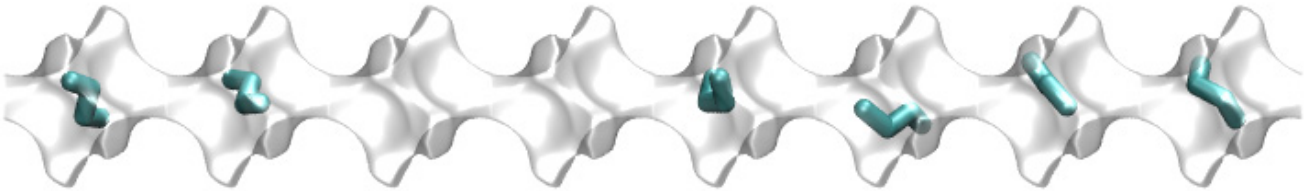

Figure S19. Snapshots showing the location of n-butane (nC4) molecules within the 1D pore landscapes of Zn(tbip) determined from CBMC simulations. The total loading is 4 molecules per unit cell.

Animations

For visual appreciation of the diffusion phenomena in Zn(tbip), animations were created on the basis of the MD simulations; these can be viewed after downloading the movies from our website (http://www.science.uva.nl/research/cr/animateMD/).

Acknowledgements

We are grateful to T.J.H. Vlugt, Delft, for providing the BIGMAC code. This code was modified to handle rigid molecular structures and charges, with generous assistance and technical inputs from S. Calero, Seville.

Table S1. Lennard-Jones parameters for atoms in metal-organic host framework for Zn(tbip). The Zn parameters are taken from the UFF force field; the other parameters are from DREIDING .

(pseudo-) atom	σ / Å	ε/k_B / K
Zn	2.69	0.41
O	3.03	48.19
C	3.47	47.86
H	2.85	7.65

References

[1] L. Pan, B. Parker, X. Huang, D.H. Olson, J.Y. Lee, J. Li, Zn(tbip) (H_2 tbip)=5-tert-Butyl Isophthalic Acid): A Highly Stable Guest-Free Microporous Metal Organic Framework with Unique Gas Separation Capability, J. Am. Chem. Soc. 128 (2006) 4180-4181.

[2] S.S.Y. Chui, S.M.F. Lo, J.P.H. Charmant, A.G. Orpen, I.D. Williams, A chemically functionalizable nanoporous material $[Cu_3(TMA)_2(H2O)_3]_n$, Science 283 (1999) 1148-1150.

[3] J.M. van Baten, R. Krishna, MD animations of diffusion in nanoporous materials, University of Amsterdam, Amsterdam, http://www.science.uva.nl/research/cr/animateMD/, 1 June 2008.

[4] D. Dubbeldam, S. Calero, T.J.H. Vlugt, R. Krishna, T.L.M. Maesen, B. Smit, United Atom Forcefield for Alkanes in Nanoporous Materials, J. Phys. Chem. B 108 (2004) 12301-12313.

[5] A.K. Rappé, C.J. Casewit, K.S. Colwel, W.A. Goddard, W.M. Skiff, UFF, a Full Periodic Table Force Field for Molecular Mechanics and Molecular Dynamics Simulations, J. Am. Chem. Soc. 114 (1992) 10024-10035.

[6] S.L. Mayo, B.D. Olafson, W.A. Goddard, DREIDING: A Generic Force Field for Molecular Simulations, J. Phys. Chem. 94 (1990) 8897-8909.

[7] D. Frenkel, B. Smit, Understanding molecular simulations: from algorithms to applications, Academic Press, 2nd Edition, San Diego, 2002.

[8] T.J.H. Vlugt, R. Krishna, B. Smit, Molecular simulations of adsorption isotherms for linear and branched alkanes and their mixtures in silicalite, J. Phys. Chem. B 103 (1999) 1102-1118.

[9] D. Dubbeldam, S. Calero, T.J.H. Vlugt, R. Krishna, T.L.M. Maesen, E. Beerdsen, B. Smit, Force Field Parametrization through Fitting on Inflection Points in Isotherms, Phys. Rev. Lett. 93 (2004) 088302.

[10] T.J.H. Vlugt, BIGMAC, University of Amsterdam, http://molsim.chem.uva.nl/bigmac/, 1 November 2000.

Supplementary Material 5: Reed-Ehrlich model

Concentration dependence represented by ϕ

In the Reed-Ehrlich model, the diffusivity results to be determined by only two quantities, namely $D(c=0)$ and a factor refelcting the concentration dependence. This factor is determined by the parameter ϕ. The influence of ϕ on the concentration dependence is illustrated by figure S20.

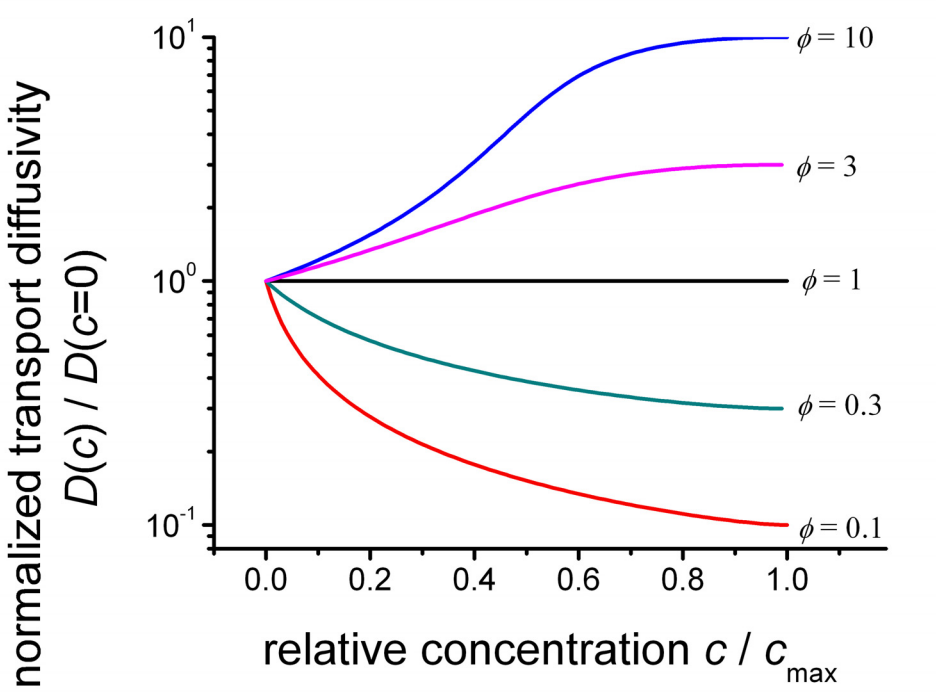

Figure S20. Transport diffusivities of a system following the Reed-Ehrlich model, as a function of the concentration for five different types of molecular interaction as provided by the parameter ϕ. The coordination number z is 2.

Results of the fit to the recorded concentration profiles

Table 1 summarizes the parameters of the Reed-Ehrlich ansatz for the diffusivities and surface permeabilities which yielded best agreement between the experimental data and the transient concentration profiles calculated by a numerical solution of the diffusion equation during ad- and desorption. In all cases (full lines in figs. 3 and S5-S7), the recalculated profiles were found to nicely reflect the measured ones. In order to provide an impression of the accuracy of the determined parameters, each single parameter was individually varied until the mean standard deviation exceeded the standard deviation of the best fit by 1 %. The resulting Reed-Ehrlich (minimum and maximum) parameters are summarized in Tab. S2. It turns out that the diffusivities and surface permeabilities at zero loading may be determined with a fairly high accuracy (± 20 %), while the Reed-Ehrlich parameter ϕ can be varied without impairing the fit dramatically.

Diffusivity						
Guest molecule	$D_0(0)$ best fit	$D_0(0)$ minimum	$D_0(0)$ maximum	ϕ_{Diff} best fit	ϕ_{Diff} minimum	ϕ_{Diff} maximum
Ethane	5.2×10^{-11} m^2 s^{-1}	4.1×10^{-11} m^2 s^{-1}	7.1×10^{-11} m^2 s^{-1}	2.6	1.3	11.4
Propane	2.4×10^{-13} m^2 s^{-1}	1.8×10^{-13} m^2 s^{-1}	3.4×10^{-13} m^2 s^{-1}	5.1	2.7	9.9
n-butane	1.3×10^{-13} m^2 s^{-1}	9.6×10^{-14} m^2 s^{-1}	1.6×10^{-13} m^2 s^{-1}	1.5	1.0	2.1
Surface permeability						
Guest molecule	$\alpha_0(0)$ best fit	$\alpha_0(0)$ minimum	$\alpha_0(0)$ maximum	ϕ_α best fit	ϕ_α minimum	ϕ_α maximum
Ethane	1.28×10^{-6} m s^{-1}	1.2×10^{-6} m s^{-1}	1.4×10^{-6} m s^{-1}	2.1	1.5	3.2
Propane	2.3×10^{-8} m s^{-1}	1.9×10^{-8} m s^{-1}	4.3×10^{-8} m s^{-1}	2.6	1.7	5.8
n-butane	7.6×10^{-9} m s^{-1}	6.4×10^{-9} m s^{-1}	8.9×10^{-9} m s^{-1}	2.1	1.4	3.1

Table S2: Maximum and minimum Reed-Ehrlich parameters which yield standard deviations which exceeded the standard deviation of the best fit by 1 %.

All profiles recorded for one type of guest molecule in one crystal have been described with the same set of parameters. Since the surface is a very unstable region of the crystal, the surface permeability might slightly vary between different experiments. For instance, the surface permeability may be influenced by impurities in the gas atmosphere. Therefore, the fitting process of the concentration profiles of the propane molecules, where more than 20 different pressure steps were fitted with only 4 parameters, was repeated with a diffusivity which is identical for all pressure steps, however, the surface permeability was independently fitted for every pressure step. In this way, a standard deviation of 3.2 % between the recorded and the recalculated concentration profiles was attained. This is slightly smaller than the results attained by only 4 fitting parameters (3.8 %).